Geolocation enhancement of spaceborne cameras: The SAR-Optic approach

Alexis Barot[1], Pascal Favé[2], Laurent Gabet[1], Mathilde Jaussaud [2], Wolfgang Koppe[3], Alain Orsoni[2], Philippe Nonin [4]

[1]Airbus Defence and Space, 5 rue des Satellites, 31030 Toulouse, France - (alexis.barot, laurent.gabet)@airbus.com
[2] IGN 6 avenue de l’Europe, 31520 Ramonville, France – (pascal.fave, mathilde.jaussaud, alain.orsoni)@ign.fr
[3]Airbus Defence and Space GmbH, Claude-Dornier-Str., 88090 Immenstaad am Bodensee, Germany - wolfgang.koppe@airbus.com
[4] Airbus Defence and Space, 2600 route des cretes, 06905 Sophia Antipolis, France – philippe.nonin@airbus.com

Keywords: Image matching, SAR, Camera orientation, Ground Control Points.

Abstract

As many observation data providers are delivering spaceborne optical images with a resolution close to airborne sources, users are expecting the same level of geolocation accuracy. Unfortunately, locating the line of sight of a camera on the ground from, at least, 500km is still a challenge. It requires a precise knowledge of the camera absolute orientation beyond current technology. Spaceborne SAR images do not suffer from this problem as the location accuracy depends only on the antenna position and speed. An operational approach is presented exploiting the geometric stability of SAR sensors to improve the location accuracy of optical images. It is based on the ability to find correspondences between overlapping SAR and optical images. The refinement of camera orientations is then achieved through photogrammetric (almost) classical techniques. A medium scale validation campaign conducted across France demonstrated an absolute horizontal geolocation accuracy of 1.5m (CE90).

1. Introduction

The geolocation accuracy of an image acquired with a spaceborne camera relies on the knowledge of the orbit of the spacecraft and the orientation of the camera. The a posteriori estimation of a satellite orbit has been a well mastered technique for a long time. Sub-meter accuracy is achievable with a reasonable effort. The geolocation, with a similar accuracy, of the line of sight of an optical instrument flying at 500 km or above is a much more challenging task. It requires expensive 3 axis attitude sensors and a fine control of the thermo-elastic behaviour of the satellite structure.
In contrast, the geolocation of a synthetic aperture radar (SAR) image depends only on the orbit of the spacecraft. Therefore, it is easier to acquire spaceborne SAR images with a sub-metric native geolocation.
The ability to find, through image matching, homologous points in SAR and optical images would transfers the native accuracy of SAR to optical observations, using classical photogrammetric bundle adjustment.

2. Geometric foreword

2.1 Geolocation accuracy

Any line of sight of a camera is determined by the six degrees of freedom (X, Y, Z, roll, pitch, yaw) of the camera frame. In SAR imagery, the geometric location of the (azimuth, range) arc is governed by the sensor's full trajectory throughout the integration time. For a well-designed spaceborne sensor, sub-meter orbital precision can be achieved a posteriori with reasonable effort. In contrast, determining the attitude (roll, pitch, yaw) of a spaceborne camera, even when using stellar sensors and high-grade gyros, cannot ensure comparable ground accuracy, at least for civilian instruments.

2.2 Bundle adjustment

In photogrammetry, bundle adjustment (or spatio-triangulation) refers to the simultaneous refinement of rays intersections and cameras orientations. It can be easily extended to other 2D imaging sensors as long as they provide a well-known differentiable projection function from the 3D space to the 2D image frame. If homologous points (projections of the same ground feature) are identified across multiple sensors images (figure 1), the relative orientations of these sensors can be mutually refined. In particular, the geolocation accuracy of optical images would benefit from the inherent geometric stability of overlapping SAR images.

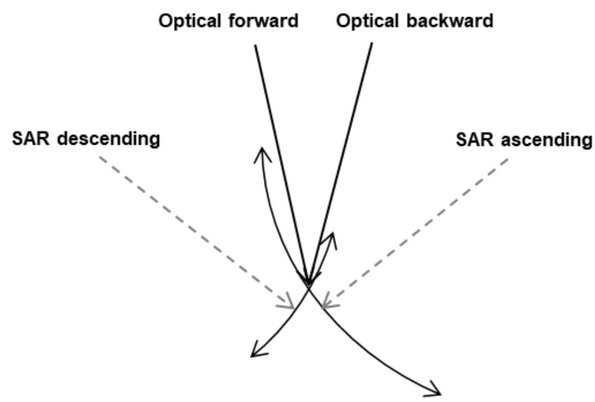

Figure 1 Intersection of optical rays with SAR wavefronts

3. SAR-Optic matching

The matching of SAR and optical imagery has been a recurring research topic for more than 35 years (Merkle, 2018). Except in very specific cases (urban structure, dry/wet fields), the matching of individual points, or small patches, between SAR and optical imagery remains practically unfeasible (figure 2). The disparity in wavelength between the two sensor types prevents any direct pixel level correlation.

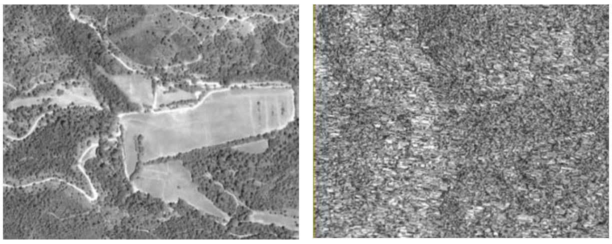

Figure 2 Same area: Optical (left) and SAR (right) images

3.1 Multi-modal images matching

At a more macroscopic level, a correspondence between SAR and optical imagery may be achievable, much like comparing MRI and X-ray images in the medical domain: By defining a parametric family of 2D transforms T_θ from image A to image B, the optimal parameter θ_{opt} can be determined using a global fitness measure between T_θ(A) and B. The mutual information is widely considered the most generic measure for such global multi-modal matching. Moreover, if mutual information proves ineffective, it is unlikely that more specialized criteria would succeed as it directly quantifies the statistical dependence between two datasets.
In practice, this approach is insufficient for matching SAR and optical images. There is no direct correlation between the electromagnetic properties of natural or man-made materials in the visible spectrum (0.5 µm) and microwave region (band X: 10 cm).

3.2 SAR-terrain correlation

There is a well-known correlation between a radar echo and the ground surface orientation: If *I* is the angle of the incident pulse with the ground surface and *R*, the reflectance of the illumined surface, the expected energy backscattered to the antenna is proportional to *R / sin(I)* (figure 3). This property was exploited more than 30 years ago for the registration of SEASAT and SIR-B images to a Digital Elevation Model (DEM) used as a reference (Rignot, 1991). Given that a DEM can be generated from a stereoscopic optical pair, we propose leveraging it as the bridge between SAR and optical domains: Since a well-defined mapping exists between the DEM grid and each optical image, registering the DEM to a SAR image establishes, by transitivity, a correspondence between the optical and the SAR imagery.

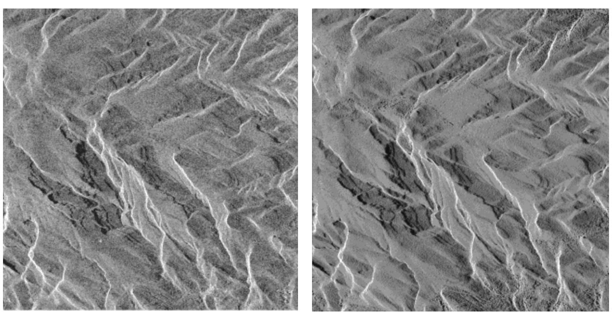

Figure 3 Real SAR image (left) and estimated backscatter based on terrain shape (right)

3.3 SAR image synthesis

From a set of overlapping optical images, we derive a 3D points cloud by stereo matching. Subsequently a synthetic SAR image is generated, simulating the expected backscatter intensity of a real SAR acquisition over the same area (figures 4, 5, 6): For each SAR pixel, the integrated backscatter is estimated from the facets of the triangulated points cloud. The simulation assumes a constant terrain reflectivity, as the actual reflectance properties are unknown. Higher order interactions such as double reflections between facades and the ground are also omitted, primarily because facades may be insufficiently represented in the 3D points cloud. At this stage, the primary objective is to produce an unbiased simulation, that avoids systematic artefacts, thereby ensuring a consistent matching process.

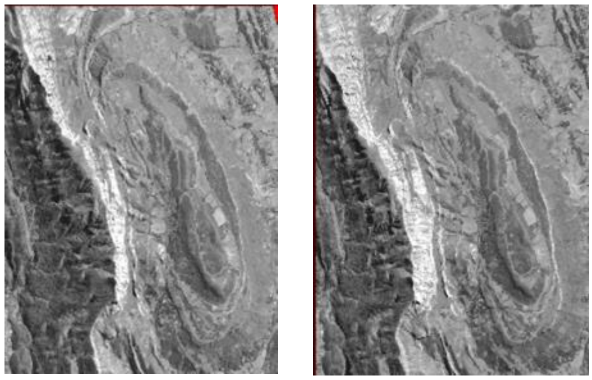

Figure 4 Optical images stereo pair (Pléiades)

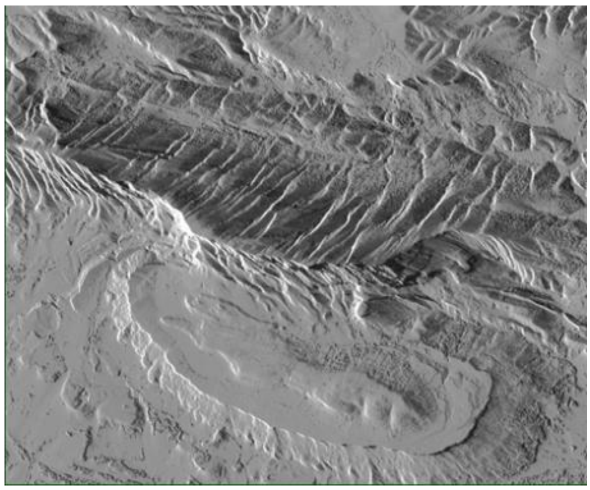

Figure 5 SAR backscatter estimation from 3D points cloud

Figure 6 Real SAR image (TerraSAR-X)

https://doi.org/10.5194/isprs-archives-XLIX-B2-2026-3-2026

3.4 Global matching

As the mis-registration of the SPOT, Pléiades and Pléiades Neo is moderate, the parametric transform between the synthetic and real SAR images is restricted to 2D affine functions.
Given the nature of the synthetic SAR image, an optimal similarity measure can be derived from the distribution of the radar signal, based on its statistical expected value (e.g. the Generalized Rayleigh distribution). This expression directly quantifies, for each pixel, the likelihood of the observed amplitude, given the simulated intensity:

$$P_a(v) = 2v^{2N-1}e^{-Nv^2/a}\frac{N^N}{(a^N(N-1)!)} \quad (1)$$

where $a = E(v^2)$ is the statistical expectation of the backscattered energy and N, the number of looks.
After a first period of experimentation, we decided to change for mutual information (also known as Kullback-Leibler divergence) which seems slightly more robust, given the limited realism of our simulation. For a given global correspondence of images A and B:

$$score = H(A) + H(B) - H(A,B) \quad (2)$$

$H(A), H(B), H(A,B)$ being, respectively the entropies and joint entropy of A, and B.
The optimal affine transform is selected through an exploration of the parameters space restricted to expected limits.

3.5 Perspectives

The relevance of the SAR-Optic matching capability must be evaluated within the operational context of the Airbus Defence and Space constellation (table 1).
Airbus commercially exploits a constellation of six optical and three SAR satellites. On the optical side, the native geolocation accuracy (CE90) ranges from 15m (SPOT6) to 3.5 m (Pléiades Neo). The SAR satellites (TerraSARX, TanDEMX and PAZ) provide, on a commercial basis, images with a (better than) 20 cm geolocation accuracy.

Name	Resolution	Accuracy	Capacity km²/day
P. Neo	0.3m	3.5m	1 M
Pléiades	0.5m	6.5m	700000
Spot	1.5m	15m	3 M
Vision1	0.9m	12m	20000
SAR (TSX, TDX, PAZ)	0.25-40m	0.1m	Up to 5.4 M (Wide ScanSAR)

Table 1 Airbus Defence and Space earth observation satellites

Launched in 2010 in collaboration with the German Aerospace Center (DLR), the TanDEM-X mission provided a global digital elevation model covering the Earth's entire land surface with a vertical accuracy better than 2m (Böer et al., 2018). The mission acquired the complete world landmass with two bi-static coverages from both ascending and descending orbits at a 3 m image resolution (Fahrland et al., 2023). This worldwide X-band bi-static archive enables global geodetic SAR applications, supported by a proven orbit accuracy exceeding 10 cm (Eineder et al., 2011).

At the same time, thanks to a partnership Airbus-IGN for the production of the 3D reference layer SRP (Chandelier, 2020), a highly redundant coverage with SPOT6/7 images has been acquired and archived. Additionally, thousands of Pléiades and Pléiades Neo stereo pairs are also available. Therefore, for any part of the world, at least two SAR images, precisely geolocated, are available for the simultaneous triangulation with a set of high-resolution optical images. This would enable the improvement of the absolute accuracy of the SRP reference from 3 m to, at least 1.5 m CE90.

4. Evaluation of SAR-Optic data

We evaluated SAR-Optic GCPs through two distinct approaches. First, we assessed the data quality by estimating the absolute geolocation accuracy of location models associated to the PLEIADES images included in each SAR-Optic package. Second, we estimated the relative accuracy of sensor models associated to SPOT images calibrated in two different bundle adjustment processes: one involves SAR-Optic data and the other one involves GNSS class GCPs, managed by the French national mapping agency.

4.1 Qualification of the absolute geolocation accuracy of SAR-Optic data

16 SAR-Optic GCPs were processed by Airbus over France metropolitan area (figure 7). They are located on landscapes specifically selected to be as much representative as possible of landscapes one can find worldwide: mountainous area with slopes suitable for DEM matching, flat rural areas where DEM matching is more challenging and urban environments where DEMs typically exhibit higher noise levels.

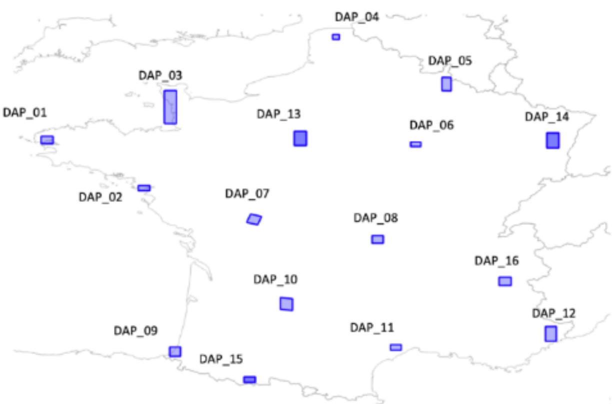

Figure 7 SAR-Optic GCPs over France

Over France, two types of reference data are available. They both offer a high level of precision:

- Orthoimages (BD Ortho) with a 50 cm resolution. Those images are handy for the identification of very precise details, with a 10 cm planimetric accuracy, exceeding the target accuracy of SAR-Optic GCPs
- Lidar DTM offering an altimetric accuracy better than 1m.

On each SAR-Optic footprint, at least 30 points were identified on reference orthoimages and on the two PHR-images of the optical component of the SAR-Optic GCPs. For each point, two sets of coordinates were computed:

- A reference set of coordinates measured on orthoimages (X, Y) and on DTM (Z).

- A set of coordinates calculated as an intersection of the lines of sight associated to the homologous positions of the GCP, identified in the PHR stereopairs.

All coordinates were computed in a common coordinates system to neutralize the effects of the plate tectonics: ITRF 2008, epoch 2018.

For each SAR-Optic area, the difference between the set of SAR-Optic points coordinates and the reference coordinates was performed. When outliers were identified, coordinates were checked and eventually excluded from the final statistics. Very few points were excluded; at least 29 points were retained at each SAR-Optic GCP.

The final assessment of SAR-Optic accuracy was performed by combining the measurements for all GCPs. The planimetric accuracy of SAR-Optic is less than 1 m (figures 8 and 9) and the altimetric accuracy of SAR-Optic is close to 1 m with a significant standard deviation (figures 10 and 11).

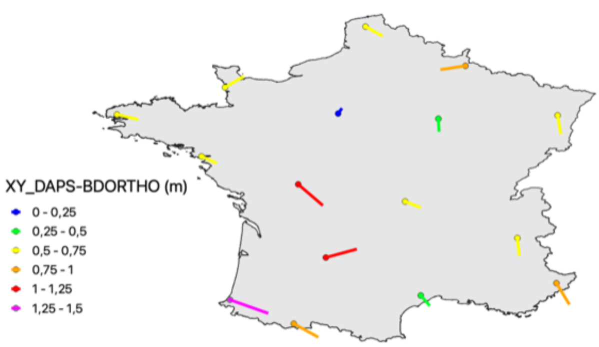

Figure 8 Planimetric accuracy of each SAR-Optic compared to IGN's references

#DAP	DX_MOY	DX_ECT	DY_MOY	DY_ECT	DXY_MOY	DXY_CE90	NB_PTS
DAPS	0.41	0.6	-0.23	0.41	0.47	1.49	491

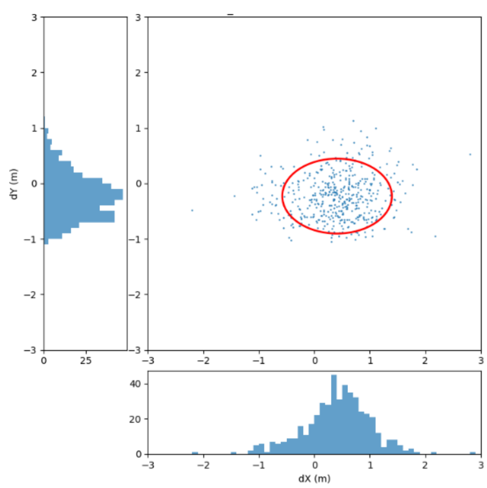

Figure 9 Statistics distribution for planimetry

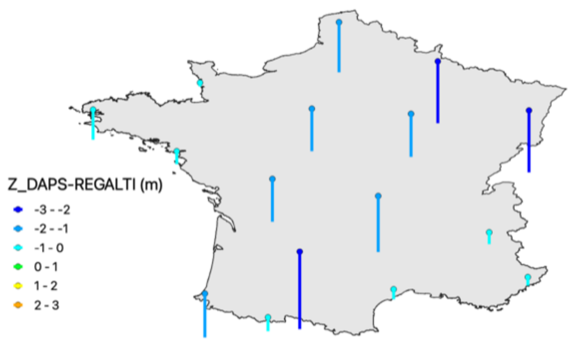

Figure 10 Altimetric accuracy of each SAR-Optic compared to IGN's references

#DAP	DZ_MOY	DZ_ECT	DZ_CE90	NB_PTS
DAPS	-1.04	1.66	3.44	491

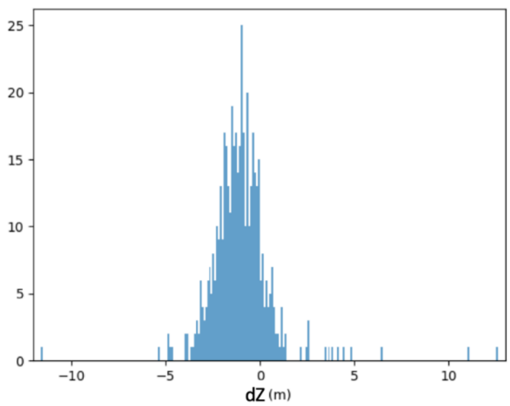

Figure 11 Statistics distribution for altimetry

The geographic representation shows that the planimetric accuracy of SAR-Optic GCPs depends on viewing acquisition conditions of the PHR stereopairs. The planimetric accuracy is better when the average acquisition angle of the two images is close to nadir.

The geographical representation of the altimetric bias shows that the highest values are distributed along a diagonal. There is no correlation with the acquisition conditions or terrain type. SAR-Optic data are less accurate on the altimetric component.

4.2 Contribution of SAR-Optic GCPs in bundle adjustment process

This validation of SAR-Optic accuracy relies on the comparison of absolute location model estimates calibrated in a different bundle adjustment process. Images involved in the process are SPOT 6 images covering the metropolitan area. Tie points are identified where SPOT6 images overlaps. The tie points reference coordinates were calculated by intersecting lines of sight using images’ location model after bundle adjustment.

A reference bundle adjustment involves GNSS class GCPs with an accuracy close to 10 cm, the contribution of SAR-Optic GCPs is compared to this reference through three other bundle adjustments.

The first bundle adjustment involves GCPs previously used in the SRP GCP production process: PHR images stacks and ICESAT points. The second uses SAR-Optic GCPs in place of PHR stacks and ICESAT points to improve image location models. The third uses SAR-Optic GCPs and ICESAT2 points as planimetric and altimetric GCPs.

For each bundle adjustment, images' locations models were updated, and SRP points coordinates were calculated. The following results present differences between each calculation of SRP coordinates with the reference coordinates which is the SRP coordinates calculated with the process based on IGN's references.

First, the difference between SRP based on IGN's references and SRP based on PHR stacks and ICESAT points shows that the actual SRP planimetric accuracy is close to 3m, as expected in the SRP specifications (table 2, figures 12 and 13).

#DAP	DX_MEAN	DX_STD	DY_MEAN	DY_STD	DXY_CE90	DZ_MEAN	DZ_STD	DZ_LE90
DAPS	0.21	0.63	-0.03	1.02	2.04	0.43	0.76	1.43

Table 2 Differences between SRP based on IGN's references and SRP based on PHR stacks and ICESAT points (actual production process)

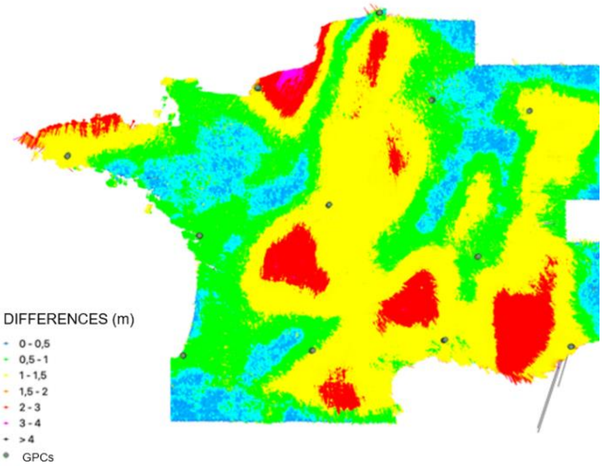

Figure 12 Geographical representation of planimetric differences

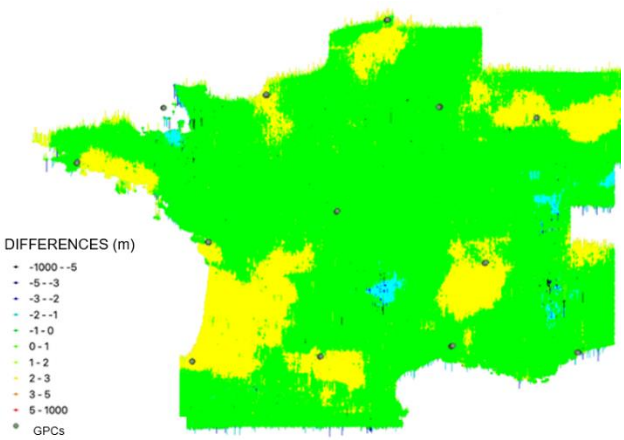

Figure 13 Geographical representation of altimetric differences

After replacing PHR image stacks and ICESAT points with the 16 SAR-Optic GCPs, a new bundle adjustment was performed from scratch. A new set of coordinates is then calculated, and the coordinates are compared to the same reference GCPs (table 3, figures 14 and 15).

#DAP	DX_MEAN	DX_STD	DY_MEAN	DY_STD	DXY_CE90	DZ_MEAN	DZ_STD	DZ_LE90
DAPS	0.4	0.59	0.17	0.48	1.33	-0.49	1.26	2.26

Table 3 Differences between SRP based on PHR stacks and ICESAT points and SRP based on SAR-Optic GCPs

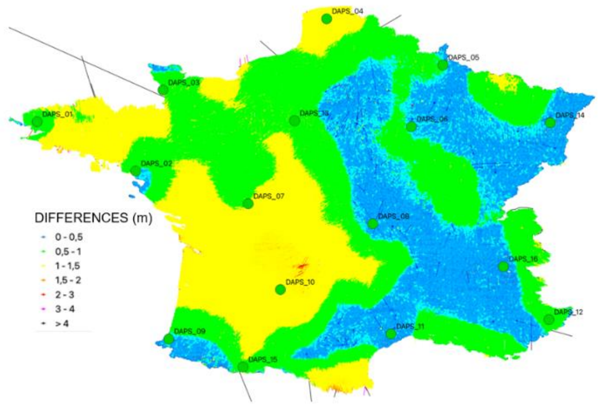

Figure 14 Geographical representation of planimetric differences

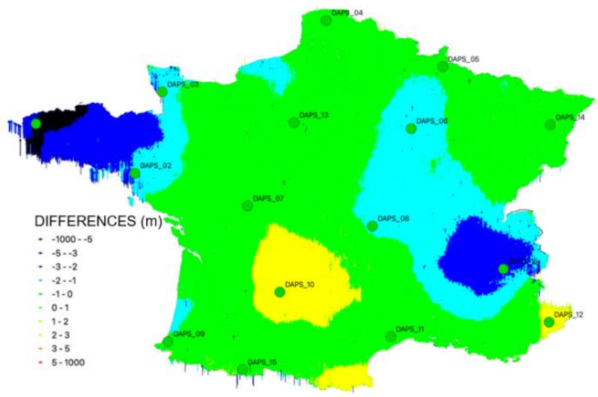

Figure 15 Geographical differences of altimetric differences

The planimetry accuracy is improved thanks to the high planimetric precision of the SAR-Optic GCPs.
But, the altimetric accuracy is yet to be improved. DZ_LE90 value of 2.26 m is worse than the previous results: DZ_LE90: 1.43 m; the standard deviation increases. These results are due to an altimetric accuracy of SAR-Optic data, which doesn't match the one of ICESAT data.

A final test was performed using 16 SAR-Optic GCPs together with ICESAT points in a bundle adjustment in order to add altimetric constraints in the process, with a homogeneous data source. Such constraints improve the altimetric accuracy without degrading the planimetric accuracy (table 4, figures 16 and 17).

#DAP	DX_MEAN	DX_STD	DY_MEAN	DY_STD	DXY_CE90	DZ_MEAN	DZ_STD	DZ_LE90
DAPS	0.28	0.5	-0.15	0.54	1.2	-0.02	0.95	1.56

Table 4 Differences between SRP based on PHR stacks and ICESAT points and SRP based on SAR-Optic GCPs and ICESAT points

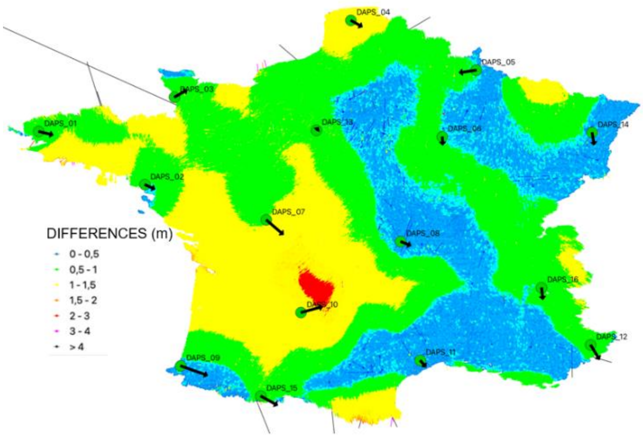

Figure 16 Geographical representation of planimetric differences

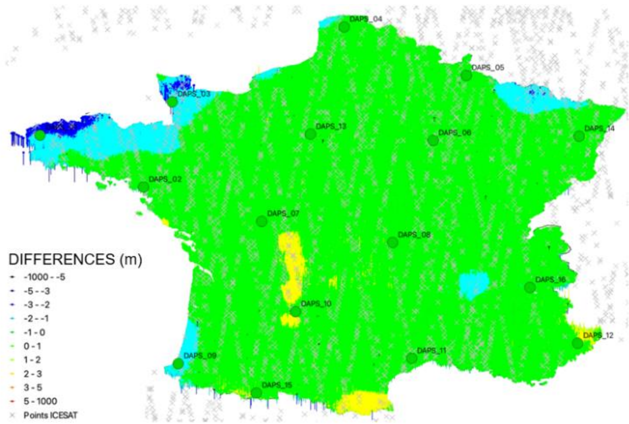

Figure 17 Geographical representation of altimetric differences

5. Conclusions

As a conclusion, we got the following accuracy of SAR-Optic GCPs estimated from 16 various landscapes over France:

- Planimetric accuracy: less than 1m
- Altimetric accuracy: close to 1m with a significant standard deviation

These results still need to be validated on two landscape types not yet studied: deserts area and dense forest.
Introduction of SAR-Optic GCPs in a bundle adjustment process contributes to the improvement of the planimetric but the use of additional data benefits is still a need to get a proper altimetric accuracy.

References

Böer, J., Wecklich, C., Bachmann, M., Buckreuss, S., Rizzoli, P., and Zink, M.: TANDEM-X mission status, products and perspectives, Int. Arch. Photogramm. Remote Sens. Spatial Inf. Sci., XLII-1, 45–49, https://doi.org/10.5194/isprs-archives-XLII-1-45-2018, 2018.

Chandelier, L., Coeurdevey, L., Bosch, S., Favé, P., Gachet, R., Orsoni, A., Tilak, T., and Barot, A.: A worldwide 3D GCP database inherited from 20 years of massive multi-satellite observations, ISPRS Ann. Photogramm. Remote Sens. Spatial Inf. Sci., V-2-2020, 15–23, https://doi.org/10.5194/isprs-annals-V-2-2020-15-2020, 2020.

Eineder, M. Minet, C. Steigenberger, P., Cong, X., and Fritz, T. Imaging geodesy - Toward centimeterlevel ranging accuracy with TerraSAR-X. IEEE Transactions on Geoscience and Remote Sensing, 49(2):661–671, 2011.

Fahrland, E., Paschko, H., Schrader, H., and Herrere, V.: Evolution of the Copernicus DEM: beyond today’s elevation data with WorldDEM Neo. Geomophometry, Romania, 2023

Merkle, Nina Marie. "Geo-localization Refinement of Optical Satellite Images by Embedding Synthetic Aperture Radar Data in Novel Deep Learning Frameworks." Doctoral thesis, 2018. https://repositorium.ub.uni-osnabrueck.de/handle/urn:nbn:de:gbv:700-20181206863.

Rignot, EJM, Kowk, R., Curlander, JC, & Pang, SS. (1991). Automated multisensory registration – Requirements and techniques. Photogrammetric Engineering and Remote Sensing 57(8), 1029-1038.